First detection of x-ray whispering gallery modes at the surface meniscus of a rotating liquid

LEONID I. GORAY,[1,2,3,*] **VIKTOR E. ASADCHIKOV,**[4] **BORIS S. ROSHCHIN,**[4] **YURI O. VOLKOV,**[4] **AND ALEKSEY M. TIKHONOV**[5,6]

[1]*Saint Petersburg Academic University, Khlopin str. 8/3, Let. 'A', St. Petersburg 194021, Russia*
[2]*ITMO University, Kronverkskiy pr. 49, St. Petersburg 197101, Russia*
[3]*Institute for Analytical Instrumentation, Rizhsky pr. 26, St. Petersburg 190103, Russia*
[4]*A. V. Shubnikov Institute of Crystallography, Leninskii pr. 59, Moscow 119333, Russia*
[5]*P. L. Kapitza Institute for Physical Problems, Kosygina str. 2, Moscow 119334, Russia*
[6]*tikhonov@kapitza.ras.ru*
[*]*lig@pcgrate.com*

Abstract: Whispering galleries propagating along large-radius concave meniscuses at the surfaces of rotating deionized water as well as hydrosol of ∼ 10 nm amorphous silica particles enriched by CsOH were probed by both x-ray reflectometry and x-ray fluorescence for the first time. The measurements were carried out at a wavelength of 1.5405 Å of Cu-K_α radiation by using a homemade diffractometer with a moving tube-sample-detector system. According to the experimental results, the x-ray beam deflection angle at the sol's surface reaches 4°, which is roughly four times higher than that obtained on the water surface. The rigorous solution of the Helmholtz equation for the whispering gallery reflection mode at the concave liquid surface agrees well with experimental observations. We attribute the difference in the x-ray beam deflection angle for the studied liquids to the difference in their viscosity, which presumably is inversely proportional to the effective surface roughness.

1. Introduction

The phenomenon of whispering gallery is based on the fact that waves in enclosed space do not propagate along the shortest path, but rather broadcast along concave walls or domes due to a guided mode generated by repeated reflections [1]. High quality factors of whispering modes enable design of extremely sensitive devices. For example, micromechanical, electromechanical and optomechanical oscillators as well as semiconductor laser micro-resonators appear to be very useful for several applications in nanotechnology, bioelectronics and optoelectronics [2–4].

In the field of x-ray optics, devices based on the whispering gallery effect are very useful as beam deflectors and polarizers [5,6]. The gallery effect was observed by Liu *et al*. on x-ray bound states trapped on a curved surface, which were realized by coupling subangstrom photons at grazing angles into a bent silicon wafer with adjustable radius [7]. Yakimchuk *et al*. reported on the whispering gallery in the hard x-ray range, which was observed on the spherical surface of a glass mirror [8]. In the experiments of Ref. [8], the authors used a very simple optical scheme consisting of an x-ray tube as a source of a divergent non-monochromatized beam and the tube window as an aperture. In this paper, we report our findings on x-ray whispering gallery waves propagating along large-radius meniscus at the concave surface of a rotating liquid. To the best of our knowledge, this is the first study on the characteristics of whispering modes propagating at a liquid surface with the use of both x-ray reflectometry and x-ray fluorescence.

2.   Experimental

The experiments were carried out under normal conditions using a handmade 'butterfly-type' x-ray diffractometer with independent movements of the x-ray source, detector and sample table [9]. The setup includes the following components: a laboratory x-ray tube at a photon energy of ~8048 eV ($\lambda \approx 1.5405$ Å); x-ray 2D (Ximea, MH110XC-KK-FA) and fluorescence (x-ray spectrometer Amptec X-123) detectors; and a motorized fluoroplastic dish with sample liquid (~ 50 ml capacity with a 100-mm-diameter circular area). The latter is mounted on the diffractometer sample table so that its center coincides with the center of rotation of the goniometer (see Fig. 1).
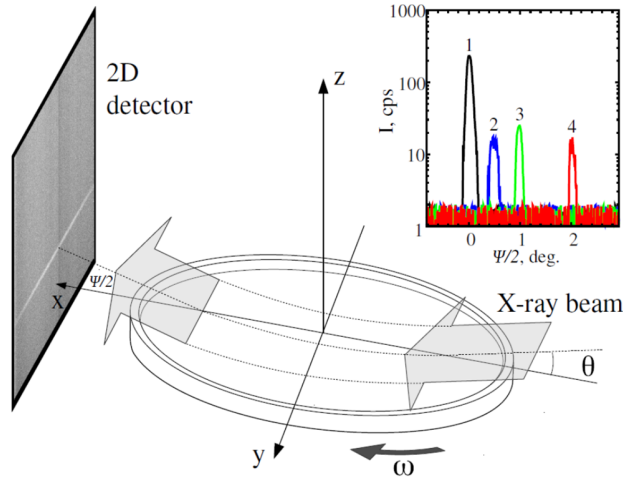

Fig. 1. Schematic the set up for probing x-ray whispering gallery modes propagating along the concave surface of the rotating liquid. The shape of the concave meniscus at the surface of the rotating liquid $z(x) = (\omega^2/2g)x^2$ is defined by the angular velocity, ω, of the rotation around Oz-axis and acceleration of gravity, g. The center of the rotation is at $x, z = 0$. Inset: integral count-rate with a noise reduction of the detector along Oy-axis as a function of the scattering angle $\psi / 2$, (1) for the direct beam; (2) for the specular reflectance from the water meniscus; (3,4) for the specular reflectances from the concave silica sol surface.

The x-ray path includes an aperture slit of 0.2 mm width, a Si111 single-crystal monochromator and two collimating slits. Upon reflection from the monochromator, the incident beam splits into a pair of $K_{\alpha 1}$ and $K_{\alpha 2}$ beams. The first collimating slit cuts off the $K_{\alpha 2}$ line and limits the divergence width of the $K_{\alpha 1}$ line. The second collimating slit partially cuts off the parasitic scattering on the first one. Thus, the probe beam with vertical width ≈ 0.1 mm and divergence $\approx 0.03°$ has a monochromaticity $\lambda / \Delta\lambda$ as high as $\approx 10^4$.

In our experiment, we used deionized water as well as hydrosol Ludox SM of ~ 10 nm silica nanoparticles (30% SiO_2 and 0.5% Na by weight) enriched by heavy alkali ions of Cs^+ with bulk concentration ~ 0.7 mol / L [10]. The level of the sample liquid in the dish was kept slightly above the edges by roughly 0.5 mm. The angle of total external reflection, θ_c, at the liquid substrate surface is defined by the bulk electron density, ρ, so that $\theta_c = \lambda\sqrt{r_e\rho/\pi}$, where $r_e = 2.814 \times 10^{-5}$ Å is the classical electron radius. Thus, for the water and the sol surfaces, the θ_c values are $\approx 0.15°$ and $\approx 0.16°$, respectively.

We start the experiment with the "beam-splitting" procedure, at which the dish with liquid sample is displaced vertically in the direction opposite to the gravity (Oz-axis) until it cuts half of the initial beam intensity at the detector. Then, the x-ray source is rotated relative to the center of the sample by an angle, θ, that is approximately half of θ_c, so that only the reflected beam is registered by the detector. As a result, the illuminated area of the sample's surface lies roughly

at its center. Furthermore, a concave surface meniscus forms due to controlled rotation of the dish in the range of angular speed from 0 to 3.6 rad / s. The shape of the concave meniscus at the surface of the rotating liquid $z(x) = (\omega^2/2g)x^2$ is defined by the angular velocity, ω, of the rotation around Oz-axis and acceleration of gravity, g. The center of the rotation is at $x, z = 0$. Rotation at a speed of 3.6 rad / s causes both shift in the beam's spot at the detector and decrease of its integral intensity by up to ten times. In order both to optimize the conditions of beam incidence with respect to the edges of meniscus and to increase the reflected intensity, manual adjustment of the sample dish height position approximately by the meniscus depth ($\sim 100~\mu$m) is required. Figure 1 schematically illustrates the reflectivity measurements and the insert to Fig. 2 — a sketch of reflection from the concave surface.
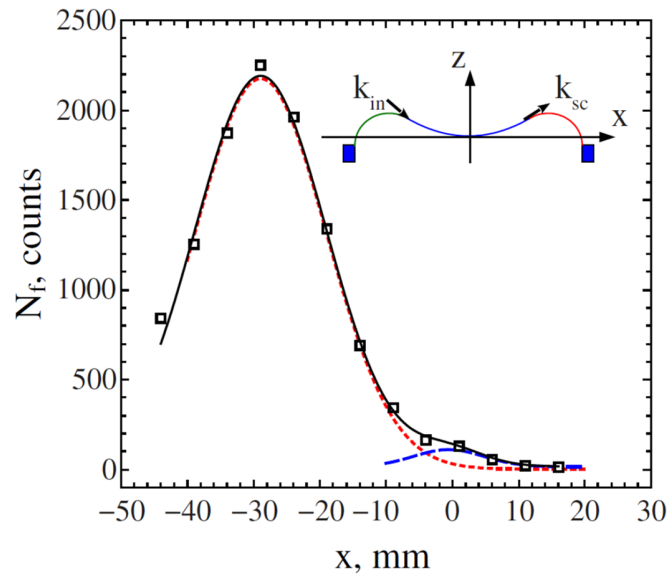

Fig. 2. Distribution of x-ray fluorescence counts at $\lambda \approx 2.892$ Å along the concave surface of the cesium-enriched hydrosol. The experimental data (squares) are approximated by two Gaussian functions (dashed lines) centered at $x \approx -30$ mm and $x \approx 0$. The solid line is the sum of the two dashed curves. Inset: scheme of reflection from the concave surface.

According to the experimental data, the x-ray beam rotation angle $\Psi~(= 2\theta)$ reaches the maximum value of $4°$ at the sol's surface while it is much lower at the water surface. As depicted in Fig. 1 (inset), the same level of the reflected intensity in the latter case is achieved at $\sim 1°$. In the data presented in Fig. 1 the detector noise has been accounted in such a way that everything outside the reflected beam was replaced by a random function ranging from zero to one. In Fig. 2, squares show data for the synchronized x-ray fluorescence measurement, which reveal the *L-α* fluorescence line for Cs$^+$ at the photon energy of 4.2865 keV ($\lambda = 2.892$ Å). The data were taken at the surface of silica sol enriched with Cs$^+$ ions at $\Psi = 4°$ by moving the fluorescence detector with Be window (7 mm in diameter at a distance ~ 5 mm from the surface) along the Ox-axis.

3. Theoretical

For quantitative analysis of x-ray scattering intensities, we have developed a hybrid model of the surface-normal structure for the upper transient layer of the liquid samples. It takes into account the following: (a) depth-graded variation of the electron density normally to the surface; (b) superposition of the stochastic capillary roughness with Gaussian height distribution and K-correlation function against the sine-shaped ripples at the air/liquid interface caused by

mechanical vibrations; (c) absorption of x-ray radiation in the transient layer at the interface. A similar rigorous approach, using the Monte Carlo technique to simulate quasi-random surfaces, was applied earlier by us to develop the models of triangular-shaped quantum dot ensembles and trapezium-shaped flight Mo/Si multilayer gratings [11,12]. We used a quasi-grating model for the surface structure caused by the surface waves and ripple near-zone ordering including thermal capillary waves and quasi-periodical surface clusters [13,14].

To account for interference effects, we model sinusoidal ripples by using a number of very thin uniform rectangular layers (slabs) [15]. The transient surface layer was divided into 146 slabs with the total layer depth of 52.7 nm. The depth of ripples was in the interval from 1 to 6 nm. Depending on the liquid type and vibration conditions, the simulated rms surface roughness σ was in the range from 0.3 to 2.0 nm. The correlation length (quasi-period) was estimated as ~ 100 nm from our atomic-force microscopy measurements of silica hydrosols surfaces as well as from the measurements of 2D clusters of polypeptide molecules [16,17].

The whispering gallery mode structure near the surface of a concave meniscus can be determined from a solution of the respective Helmholtz equation. The asymptotics of such glancing incidence waves are mostly determined by the property of Airy functions near the zeros (for example, see [18]). In cases of small roughness ($\sigma \leq 10$ nm) and sufficiently large meniscus radius (> 5 cm), x-ray radiation losses can be ignored. Then, the reflectance accounting for quadratic terms on the grazing incidence angle θ, that may be significant in the considered cases, is determined for the rotation angle, ψ, as follows:

$$R(\theta, r, \psi) = I_0(\theta, r, 0) exp\left\{-2\psi Re\left[\frac{\eta}{\sqrt{\varepsilon - 1}} - \frac{\theta\eta^2}{\varepsilon - 1}\right]\right\}, \tag{1}$$

where $I_0(\theta, r, 0)$ is the incident intensity expressed in cylindrical coordinates, $\eta = 1$ or $\eta = \varepsilon$ for TE or TM polarization, respectively, and $\varepsilon = 1 - \delta + i\gamma$. For a low-absorbing regime $\gamma << \delta$ (in our case, $\gamma / \delta \sim 10^{-3}$) and close to zero-angle incidence, the reflectance can be calculated using the known expression obtained for TE polarization [4]:

$$R(\theta, r, \psi) = I_0(\theta, r, 0) \exp\left\{-2\psi Im\left[\frac{1}{\sqrt{1 - \epsilon}}\right]\right\}. \tag{2}$$

The structure of the air/water and air/sol interfaces was studied earlier by others with x-ray reflectivity measurements [19–21]. The surface-normal structure of the former is described by only one parameter, that is surface capillary-wave roughness, σ_{capil}. The structure of the latter is more complex and represented by a layer of suspended Cs^+ ions with their maximum concentration near the surface and a layer of SiO_2 particles positioned at a depth of ~ 15 nm from the sol's surface. It reflects the difference between the potentials of electrical image forces for alkali cations and nanoparticles (macroions) [22].

Thus, the profile for the real part $\delta(z)$ of $\varepsilon(z)$ in the upper non-uniform layer was derived from the reflectometric measurements of electron density distributions, while the imaginary part $\gamma(z)$ was calculated using the atomic scattering factors [23]. To describe the effective surface roughness, σ_{eff}, which includes sine-shaped ripples, for both air/water and air/sol interfaces, we applied the hybrid model, where

$$\sigma_{eff}^2 = \sigma_{capil}^2 + \sigma_{fract}^2. \tag{3}$$

The capillary rms roughness, σ_{capil}, describes the influence of temperature-activated fluctuations at the surface, while the fractal roughness, σ_{fract}, describes the effect of vibrations caused by the motor drive.

According to the theory and experimental data available in literature, the values of σ_{capil} for the flat H_2O surface and silica sol surface are almost the same ~ 0.3 nm. [20,24–27]. This is

defined by the surface tension, τ, the values of which are almost the same for silica hydrosol ($\tau \approx$ 74 mN / m) and water ($\tau \approx 72$ mN / m) [19].

To determine the scattering intensity, we used numerical calculations based on the rigorous method of boundary integral equations developed, in particular, to analyze x-ray randomly rough multilayer mirrors and gratings [12,28,29]. To compute the model, we used the PCGrates-SX v. 6.7 commercial code [30]. The rigorous approach allows precise accounting for the electron density (refractive indices) varying in the upper layer, quasi-random sine ripples, absorption and polarization. In our theoretical model, the capillary roughness of the interface, as well as the thicknesses and refractive indices of the layers, were not fitted numerically, but were adopted from our previous measurements and/or respective computations for the flat surfaces of stationary liquid samples, and then incorporated into the rigorous solution of Maxwell's equations.

4. Results and discussion

The applicability of our theoretical model can be tested by its comparison with our previous measurements of specular reflectivity from the flat surfaces of cesium-enriched hydrosols, namely, solutions Ludox SM of ~ 10-nm particles and Ludox FM of ~ 7-nm particles (16% of SiO_2 and 0.3% of Na by weight) with cesium bulk concentration ~ 0.7-0.9 mol / L [27]. The solid lines in Fig. 3 represent the specular reflectivity from the air/sol surfaces calculated using the hybrid model. The dotted lines in this figure show our previous calculations using the model-independent approach [27]. The calculations demonstrate a very good agreement with the experimental data over a wide range of incident angles; hence, we conclude that the model considers sinusoidal ripples superimposed by random roughness reasonably well.
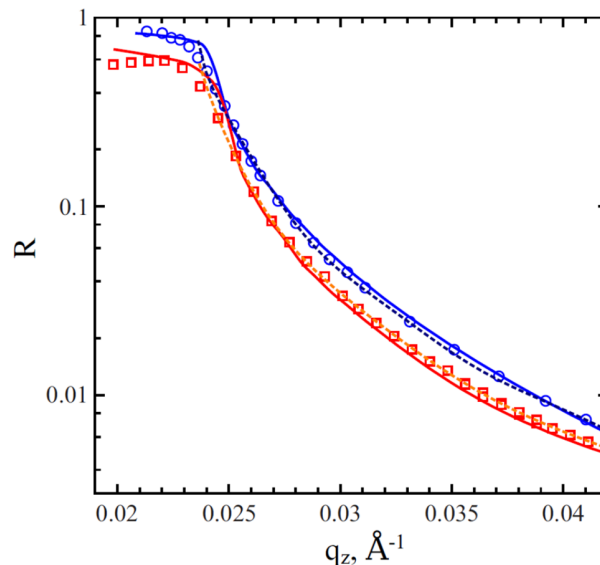

Fig. 3. X-ray reflectivity, *R*, as a function of the wave vector component, $q_z = (4\pi/\lambda)sin\theta$, normal to the surface of the cesium-enriched colloidal solution: dots represent the solution Ludox SM of ~ 10-nm particles; circles are for the solution Ludox FM of ~ 7-nm particles. Cesium bulk concentration in the sols ~ 0.7 mol / L. Solid lines correspond to the hybrid model discussed in the text. Dotted lines indicate calculation results using the model-independent approach [27].

Fitting the fluorescence emission curve using a gaussian multi-peak approach (solid line in Fig. 2) reveals two characteristic maxima (dashed lines in Fig. 2). The first one centered at $x \approx$

–30 mm corresponds to the entry point of the x-ray beam near the edge of the concave meniscus. The second maximum at $x \approx 0$ mm roughly corresponds to the center of the meniscus at the sample's surface. The ratio of the maxima of the fluorescence peak intensity (≈ 17) coincides approximately with the ratio of the intensities maxima (≈ 17) of the incident and reflected beams at $\Psi = 4°$ (see Fig. 1, inset). We note that the characteristic propagation length along the surface per one reflection (≈ 4 mm) $>> \lambda$, so that an approximation of ray optics can be applied to describe the propagation regime of whispering waves [18]. The second maximum of the fluorescence intensity at $x = 0$ demonstrates that x-rays glancing along the surface at different depths and at slightly different angles converge near the center of the concave meniscus.

To detect both reflection and fluorescence in x-ray whispering modes, the angle of incidence, θ, (see Fig. 1) should be in the range from slightly above zero to a value less than the critical angle, $\theta_c \approx 0.16°$, for the hydrosol. Taking into account both the position of the beam incidence entry point (30 mm away from the center of the dish) and the angular velocity of rotation ($\omega \sim 3.6$ rad / c), the estimated angle between the beam and the tangent to the hydrosol surface (see Fig. 1) at the entry point appears to be about $\sim 0.15°$. This value is within the required range.

The simulated specular reflectance peak of whispering modes propagating along a concave H_2O surface is destroyed almost completely for a $1°$ rotation (4 successive reflections in total along the meniscus) due to strong ripples ($\sigma_{eff} \sim 6$ nm). Such behavior is in a good agreement with the reflectance measurements and caused by both motor drive vibrations and the presumably low viscosity of H_2O (~ 0.9 cP). In comparison with the water surface, the reflectance of whispering modes propagating near the Ludox SM surface is stronger. The parameter, σ_{eff}, in the model accounting for roughness rigorously is approximately 1.2 nm. Thus, it allows a $4°$ rotation with 14 successive reflections in total. The experimental data matched perfectly the theoretical curves calculated for the hybrid model at the critical angle of $\sim 0.16°$ (see Fig. 4). Thus, our numerical results for the reflectance, R, are in good agreement with the experimental data. In addition, an exit of grazing incidence x-ray fluorescence by Cs^+ ions (the L-α fluorescence line with the energy of 4.29 keV) suspended at the hydrosol surface was demonstrated (Fig. 2).

In Fig. 5, the complete set of the measured data of whispering gallery reflectances without a detector noise reduction is demonstrated together with the incident beam intensity. The integral count-rate along Oy-axis is presented as a function of the scattering angle $\psi / 2$ (number of multiple successive reflections at some incidence angle) from the concave silica sol surface. Thus, the maximal x-ray beam rotation angle is $4°$ for the silica hydrosol sample at Cu-$K\alpha$ radiation.

The dynamic viscosity, η, of the Ludox SM sol is 5.7 cP that is approximately six times higher than the viscosity of water under normal conditions ~ 0.9 cP [31,32]. In the first approximation, we may suppose that σ_{fract} is inversely proportional to η ($\sigma_{fract} = K / \eta$), where the proportionality constant, K, is defined by the viscosity of water and the fractal roughness of water ripples $\sigma_{fract} \sim 6$ nm. Thus, this rough estimation gives the value ~ 5.4 cP for the viscosity of the hydrosol Ludox SM that matches well the tabulated value. In order to determine the viscosity from our experiment independently, the proportionality constant K needs to be redefined in further systematic reflectometry investigations of σ_{eff} for various hydrosols under constant vibrational conditions.
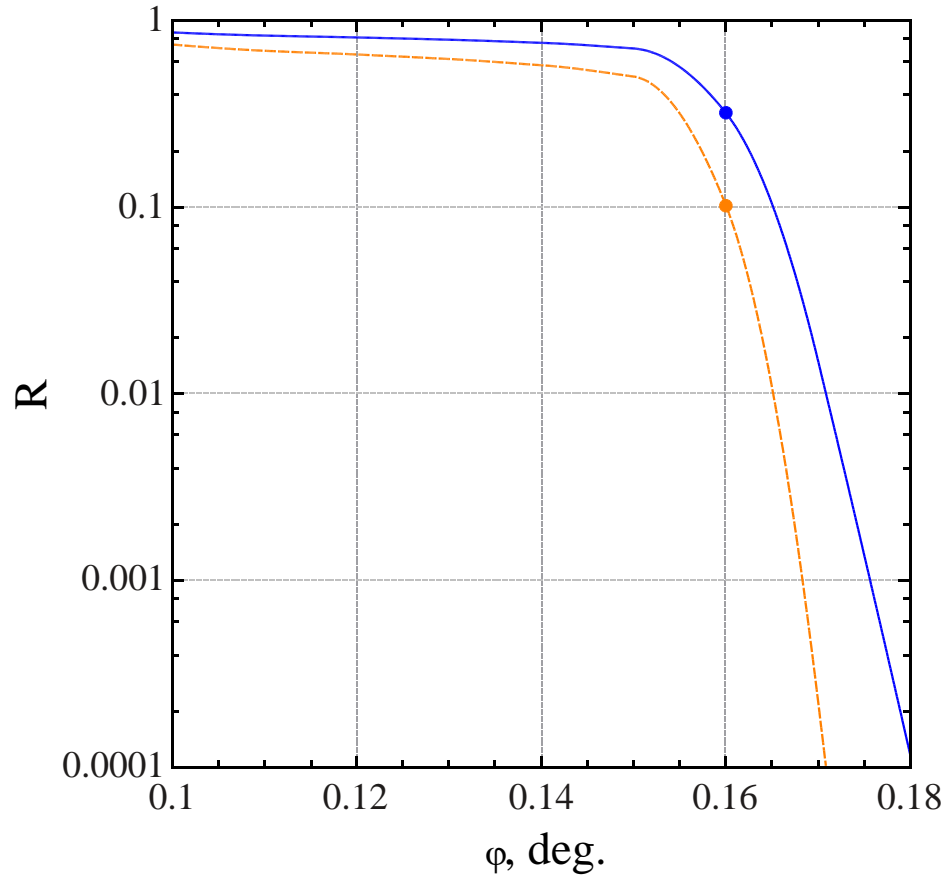
Fig. 4. Specular reflectance, *R*, for the meniscus of the cesium-enriched hydrosol Ludox SM as a function of the grazing incidence angle φ between a tangential plane to the hydrosol surface and the direction of incidence. Solid line represents calculations for the rotation angle $\Psi = 2°$. Dashed line corresponds to calculations for $\Psi = 4°$. Dots depict experimental data, which correspond to the insert in Fig. 1 with a detector noise reduction.
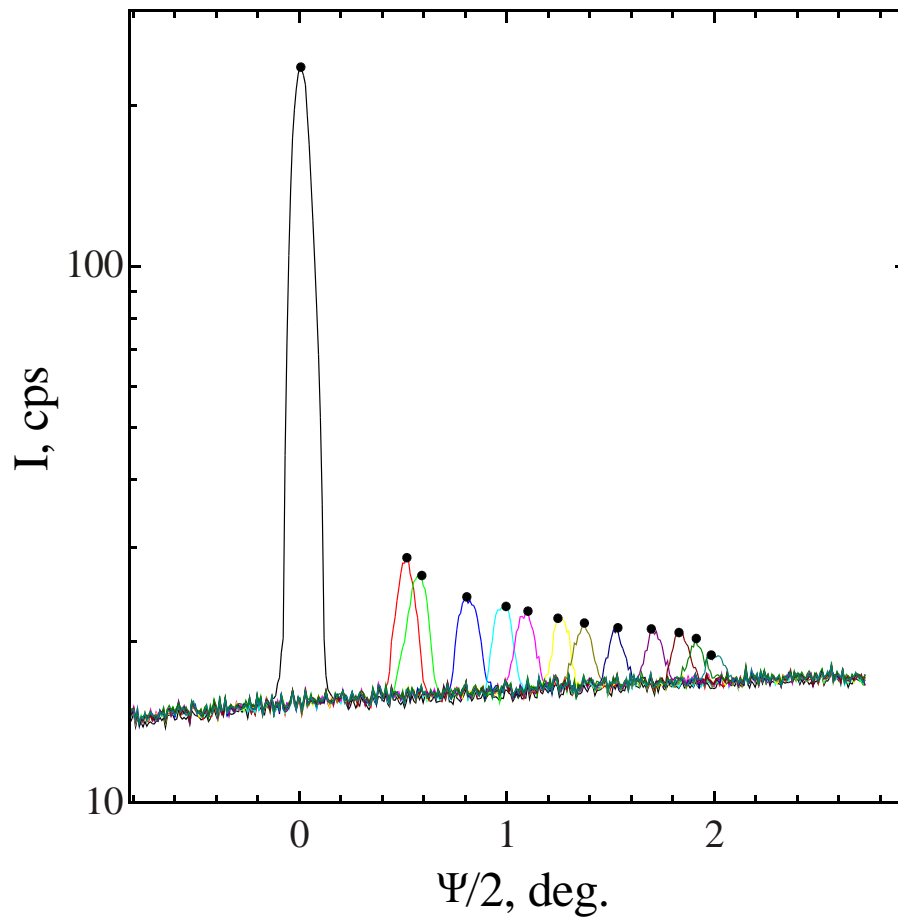
Fig. 5. Integral count-rate accounting a noise of the detector along Oy-axis as a function of the scattering angle $\psi / 2$, (highest black curve) for the direct beam; (various color shapes) for the multiple successive reflections from the concave silica sol surface.

5. Summary

In summary, we investigated for the first time the diffraction of x-ray whispering gallery waves, which propagate along large-radius concave liquid meniscuses, both experimentally and theoretically. We found that the whispering effects are more pronounced at the hydrosol substrate than at the water surface that makes the former more useful for future studies and applications. For instance, it can be applied in x-ray beam deflecting devices with continuous adjustment by the deviation angle and also in some kind of resonance fluorescence spectroscopy. We relate this observation to both the larger value of the critical angle and smaller value of fractal roughness at the sol's surface. Besides, we attribute the latter to the difference in dynamic viscosity of water and sol that presumably is inversely proportional to the effective surface roughness. The smaller value of σ_{eff} for the sol (higher viscosity) than for water (lower viscosity), explains lesser intensity losses on diffuse scattering at the sol's surface.

References

1. J. W. Strutt (Lord Rayleigh), "The problem of the whispering gallery," Philosophical magazine **20**(120), 1001–1004 (1910).
2. K. J. Vahala, "Optical microcavities," Nature **424**(6950), 839–846 (2003).
3. M. R. Foreman, J. D. Swaim, and F. Vollmer, "Whispering gallery mode sensors," Adv. Opt. Photonics **7**(2), 168–240 (2015).
4. N. V. Kryzhanovskaya, M. V. Maximov, and A. E. Zhukov, "Whispering-gallery mode microcavity quantum-dot lasers," Quantum Electron. **44**(3), 189–200 (2014).
5. I. N. Bukreeva, I. V. Kozhevnikov, and A. V. Vinogradov, "Whispering gallery mirrors for the soft x-ray region: Properties and applications," J. X-Ray Sci. Technol. **5**(4), 397–419 (1995).
6. E. Spiller, *Soft x-ray Optics* (SPIE, Bellingham, Washington, 1994).
7. C. Liu and J. A. Golovchenko, "Surface Trapped X Rays: Whispering-Gallery Modes at $\lambda = 0.7$ Å," Phys. Rev. Lett. **79**(5), 788–791 (1997).
8. I. V. Yakimchuk, B. S. Roshchin, I. V. Kozhevnikov, V. E. Asadchikov, and Zh. Wang, "Study of the whispering gallery effect on a spherical surface in the hard x-ray region," Crystallogr. Rep. **53**(6), 1054–1060 (2008).
9. V. E. Asadchikov, A. V. Buzmakov, V. N. Zryuev, Yu. S. Krivonosov, B. V. McHedlishvili, R. A. Senin, Yu. N. Shilin, V. A. Shishkov, V. G. Babak, Yu. P. Dorokhin, I. P. Glagolev, V. F. Mamich, V. D. Fateev, Yu. V. Zanevskii, L. P. Smykov, S. P. Chernenko, G. A. Cheremukhina, L. A. Moseiko, N. I. Moseiko, S. V. Savel'ev, G. A. Tudosi, E. A. Cheremukhin, and A. I. Chulichkov, "An x-ray diffractometer with a mobile emitter-detector system," Instrum. Exp. Tech. **48**(3), 364–372 (2005).
10. A. M. Tikhonov, "Ion-size effect at the surface of a silica hydrosol," J. Chem. Phys. **130**(2), 024512 (2009).
11. L. I. Goray, N. I. Chkhalo, and G. E. Tsyrlin, "Determining angles of incidence and heights of quantum dot faces by analyzing x-ray diffuse and specular scattering," Tech. Phys. **54**(4), 561–568 (2009).
12. L. I. Goray and G. Schmidt, "Boundary Integral Equation Methods for Conical Diffraction and Short Waves," in *Gratings: Theory and Numerical Applications*, E. Popov, ed., 2nd rev. ed. (Presses Universitaires de Provence, AMU, 2014). Chap. 12.
13. B. M. Ocko, in *Spectroscopic and Diffraction Techniques in Interfacial Electrochemistry*, C. Gutiérrez and C. Melendres, eds. (NATO ASI Series, 1990), p. 343.
14. M. Fukuto, R. K. Heilmann, P. S. Pershan, J. A. Griffiths, S. M. Yu, and D. A. Tirrell, "X-Ray Measurements of Noncapillary Spatial Fluctuations from a Liquid Surface," Phys. Rev. Lett. **81**(16), 3455–3458 (1998).
15. J. F. Seely, L. I. Goray, W. R. Hunter, and J. C. Rife, "Thin-film interference effects on the efficiency of a normal-incidence grating in the 100–350-Å wavelength region," Appl. Opt. **38**(7), 1251–1258 (1999).
16. A. E. Muslimov, private communication.
17. P. S. Pershan, "Effects of thermal roughness on x-ray studies of liquid surfaces," Colloids Surf., A **171**(1-3), 149–157 (2000).

18. V. M. Babich and V. S. Buldyrev, *Asymptotic Methods in Short-Wavelength Diffraction Theory* (Alpha Science, Oxford, 2007).

19. A. M. Tikhonov, "Compact Layer of Alkali Ions at the Surface of Colloidal Silica," J. Phys. Chem. C **111**(2), 930–937 (2007).

20. A. Braslau, M. Deutsch, P. S. Pershan, A. H. Weiss, J. Als-Nielsen, and J. Bohr, "Surface Roughness of Water Measured by X-Ray Reflectivity," Phys. Rev. Lett. **54**(2), 114–117 (1985).

21. V. E. Asadchikov, V. V. Volkov, Yu. O. Volkov, A. Dembo, I. V. Kozhevnikov, B. S. Roshchin, D. A. Frolov, and A. M. Tikhonov, "Condensation of silica nanoparticles on a phospholipid membrane," JETP Lett. **94**(7), 585–587 (2011).

22. A. M. Tikhonov, "Water Density in the Electric Double Layer at the Insulator/Electrolyte Solution Interface," J. Phys. Chem. B **110**(6), 2746–2750 (2006).

23. The Center of x-ray Optics, http://henke.lbl.gov/ (2018).

24. F. P. Buff, R. Lovett, and F. H. Stillinger Jr., "Interfacial Density Profile for Fluids in the Critical Region," Phys. Rev. Lett. **15**(15), 621–623 (1965).

25. A. Braslau, P. S. Pershan, G. Swislow, B. M. Ocko, and J. Als-Nielsen, "Capillary waves on the surface of simple liquids measured by x-ray reflectivity," Phys. Rev. A **38**(5), 2457–2470 (1988).

26. D. K. Schwartz, M. L. Schlossman, E. H. Kawamoto, G. J. Kellogg, P. S. Pershan, and B. M. Ocko, "Thermal diffuse x-ray-scattering studies of the water-vapor interface," Phys. Rev. A **41**(10), 5687–5690 (1990).

27. A. M. Tikhonov, V. E. Asadchikov, Yu. O. Volkov, B. S. Roshchin, V. Honkimäki, and M. V. Blanco, "Model-Independent X-Ray Scattering Study of a Silica Sol Surface," JETP Lett. **107**(6), 384–389 (2018).

28. L. I. Goray, "Application of the rigorous method to x-ray and neutron beam scattering on rough surfaces," J. Appl. Phys. **108**(3), 033516 (2010).

29. L. I. Goray, A. Yu, and Egorov, "Breaking the efficiency limit for high-frequency blazed multilayer soft x-ray gratings: Conical vs classical diffraction," Appl. Phys. Lett. **109**(10), 103502 (2016).

30. The PCGrate software, http://www.pcgrate.com/ (2018).

31. The Grace products, https://grace.com/catalysts-and-fuels/en-us/Pages/ludox-emission-control.aspx (2018).

32. E. D. Giuseppe, A. Davaille, E. Mittelstaedt, and M. Francois, "Rheological and mechanical properties of silica colloids: from newtonian liquid to brittle behaviour," Rheol. Acta **51**(5), 451–465 (2012).